Variable Step-Size Matrix for the Improved Multiband-Structured Subband Adaptive Filter

Yan Zhenhai, Yang Feiran, and Yang Jun
Key Laboratory of Noise and Vibration Research
Institute of Acoustics, Chinese Academy of Sciences
Beijing 100190, China
yanzhenhai@mail.ioa.ac.cn, feirany.ioa@gmail.com, jyang@mail.ioa.ac.cn

***Abstract*—The improved multiband-structured subband adaptive filter (IMSAF) algorithm could enhance the convergence performance of multiband-structured subband adaptive filter algorithms and affine projection. However, the original IMSAF algorithm with a fixed step-size factor have to compromise between convergence rate and steady-state misalignment. A new IMSAF algorithm with variable step-size matrix (VSM) is proposed to address this problem. The power of the subband *a posteriori* error is set to equal the power of the subband noise to deduce the formula for VSM. Two real-time noise power estimation methods are utilized to calculate the step size. Simulation results demonstrate that the new algorithms can achieve better performance both in convergence rate and steady-state misalignment than the original IMSAF algorithm with a fixed step-size factor.**

***Index Terms*—Adaptive filter, improved multiband-structured subband adaptive filter (IMSAF), variable step-size matrix**

I. Introduction

Adaptive filtering is widely utilized for many applications, such as channel equalization and acoustic echo cancellation (AEC). For input signals that have a large condition number, subband adaptive filtering algorithms have advantages in convergence performance. However, the aliasing and band-edge effects degrade the convergence rate of traditional subband adaptive filters [1]. To address this problem, a multiband method that the weighted combination of the subband input signals adjusted the fullband tap weights was proposed [2]–[5]. An improved multiband-structured subband adaptive filter (IMSAF) [6] algorithm was recently presented to deal with colored signals and long impulse responses. In [7], the IMSAF algorithm for transient and steady-state was analyzed in detail.

Similar to other LMS-type adaptive filtering algorithms, step-size factor will obviously affect the convergence performance of the original IMSAF algorithm. The step size results in a conflict between convergence rate and steady-state misalignment. Inspired by [8], we propose a method of variable step-size matrix (VSM) to address this problem. The central idea is that the power of the subband *a posteriori* error is set to equal the power of the subband noise. Consequently, different step sizes can be assigned to different subbands. Two real-time estimation methods [9], [10] are adopted to estimate the power of the subband noise. The performance of the proposed approach will be evaluated by computer simulations.

II. Review of the IMSAF Algorithm

The desired signal $d(n)$ can be modeled as follows

$$d(n) = \mathbf{w}_{\mathrm{o}}^T \mathbf{u}(n) + v(n) \tag{1}$$

where $\mathbf{w}_{\mathrm{o}} = [w_0, w_1, \cdots, w_{L-1}]^T$ is the vector of the echo path system $\mathrm{W_o}(z)$, $\mathbf{u}(n) = [u(n), u(n-1), \cdots, u(n-L+1)]^T$ indicates the far-end signal, and $v(n)$ is the near-end noise.

The signal flow graph of the IMSAF algorithm is shown in Fig. 1 [6]. $H_i(z)$ and $F_i(z)$ are respectively the analysis and synthesis filter banks. $\hat{\mathrm{W}}(z)$ is the fullband adaptive filter. $\uparrow N$ and $\downarrow N$ denote *N*-fold interpolation and decimation. z^{-1} represents a unit delay. P represents the projection order. The definitions of input signal $\mathbf{U}(k)$, desired signal $\mathbf{d}_{\mathrm{D}}(k)$, the *a priori* error signal $\mathbf{e}_{\mathrm{D}}(k)$, and the *a posteriori* error signal $\boldsymbol{\xi}_{\mathrm{D}}(k)$ are [11]

$$\mathbf{U}(k) = [\mathbf{U}_0(k), \mathbf{U}_1(k), \cdots, \mathbf{U}_{N-1}(k)], \tag{2}$$

$$\mathbf{d}_{\mathrm{D}}(k) = \left[\mathbf{d}_{0,\mathrm{D}}^T(k), \mathbf{d}_{1,\mathrm{D}}^T(k), \cdots, \mathbf{d}_{N-1,\mathrm{D}}^T(k)\right]^T, \tag{3}$$

$$\begin{aligned}\mathbf{e}_{\mathrm{D}}(k) &= \left[\mathbf{e}_{0,\mathrm{D}}^T(k), \mathbf{e}_{1,\mathrm{D}}^T(k), \cdots, \mathbf{e}_{N-1,\mathrm{D}}^T(k)\right]^T \\ &= \mathbf{d}_{\mathrm{D}}(k) - \mathbf{U}^T(k)\hat{\mathbf{w}}(k),\end{aligned} \tag{4}$$

$$\begin{aligned}\boldsymbol{\xi}_{\mathrm{D}}(k) &= \left[\boldsymbol{\xi}_{0,\mathrm{D}}^T(k), \boldsymbol{\xi}_{1,\mathrm{D}}^T(k), \cdots, \boldsymbol{\xi}_{N-1,\mathrm{D}}^T(k)\right]^T \\ &= \mathbf{d}_{\mathrm{D}}(k) - \mathbf{U}^T(k)\hat{\mathbf{w}}(k+1)\end{aligned} \tag{5}$$

where

$$\mathbf{U}_i(k) = [\mathbf{u}_i(k), \cdots, \mathbf{u}_i(k-P+1)], \tag{6}$$

$$\mathbf{d}_{i,\mathrm{D}}(k) = [d_{i,\mathrm{D}}(k), \cdots, d_{i,\mathrm{D}}(k-P+1)]^T, \tag{7}$$

$$\begin{aligned}\mathbf{e}_{i,\mathrm{D}}(k) &= \left[e_{i,\mathrm{D}}(k), \cdots, e_{i,\mathrm{D}}^{(P-1)}(k)\right]^T \\ &= \mathbf{d}_{i,\mathrm{D}}(k) - \mathbf{U}_i^T(k)\hat{\mathbf{w}}(k),\end{aligned} \tag{8}$$

$$\begin{aligned}\boldsymbol{\xi}_{i,\mathrm{D}}(k) &= \left[\xi_{i,\mathrm{D}}(k), \cdots, \xi_{i,\mathrm{D}}^{(P-1)}(k)\right]^T \\ &= \mathbf{d}_{i,\mathrm{D}}(k) - \mathbf{U}_i^T(k)\hat{\mathbf{w}}(k+1).\end{aligned} \tag{9}$$

The updated formula of the IMSAF algorithm is [6]

$$\hat{\mathbf{w}}(k+1) = \hat{\mathbf{w}}(k) + \mu\mathbf{U}(k)\left[\mathbf{U}^T(k)\mathbf{U}(k) + \delta\mathbf{I}\right]^{-1}\mathbf{e}_{\mathrm{D}}(k). \tag{10}$$

Reference [11] proved that the matrix $\mathbf{U}^T(k)\mathbf{U}(k)$ can be simplified to a block diagonal matrix without degrading the

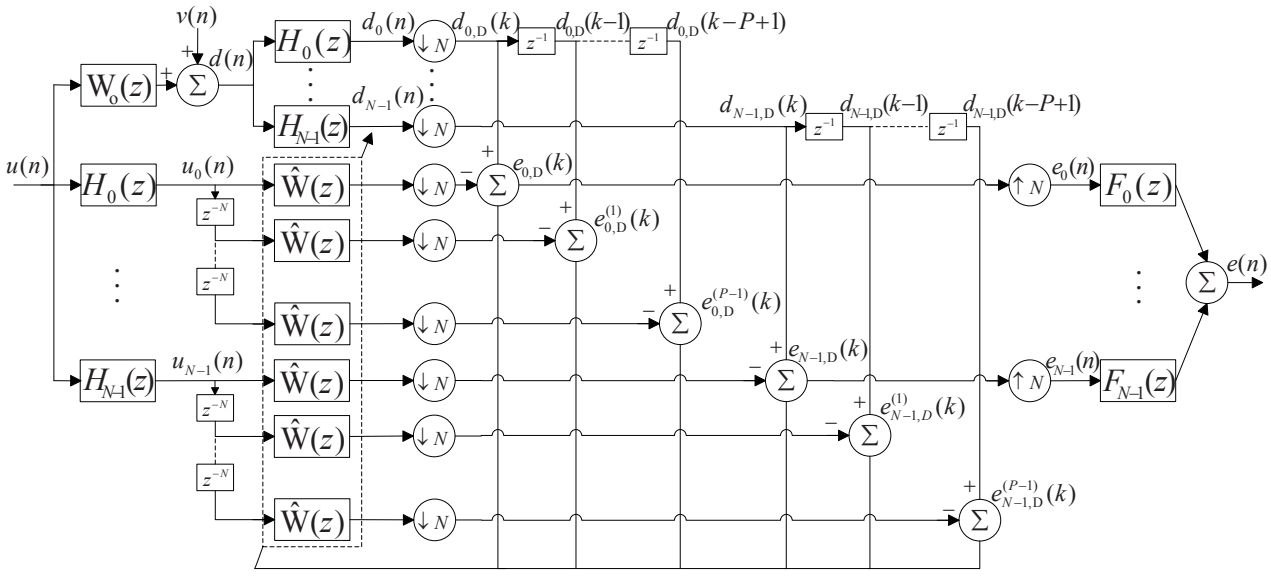

Fig. 1. Block diagram of the IMSAF algorithm.

performance significantly. Therefore, the updated formula (10) can be rewritten as [11]

$$\begin{aligned}\hat{\mathbf{w}}(k+1) = \hat{\mathbf{w}}(k) + \mu \sum_{i=0}^{N-1} \mathbf{U}_i(k) \\ \times \left[\mathbf{U}_i^T(k)\mathbf{U}_i(k) + \delta\mathbf{I}\right]^{-1}\mathbf{e}_{i,\mathrm{D}}(k).\end{aligned} \tag{11}$$

Subsequently, (11) is adopted to establish the variable step-size scheme for the IMSAF algorithm.

III. Proposed VSM-IMSAF algorithm

A. Derivation of the VSM

A variable individual step size is assigned to each subband. Then, (11) becomes

$$\begin{aligned}\hat{\mathbf{w}}(k+1) = \hat{\mathbf{w}}(k) + \sum_{i=0}^{N-1} \mu_i(k)\mathbf{U}_i(k) \\ \times \left[\mathbf{U}_i^T(k)\mathbf{U}_i(k) + \delta\mathbf{I}\right]^{-1}\mathbf{e}_{i,\mathrm{D}}(k)\end{aligned} \tag{12}$$

where $\mu_i(k)$ represents the step-size factor of the ith subband. In Fig. 1, the subband desired signal vector can be written as

$$\mathbf{d}_{i,\mathrm{D}}(k) = \mathbf{U}_i^T(k)\mathbf{w}_{\mathrm{o}} + \mathbf{v}_{i,\mathrm{D}}(k) \tag{13}$$

where $\mathbf{v}_{i,\mathrm{D}}(k) = [v_{i,\mathrm{D}}(k), v_{i,\mathrm{D}}(k-1), \cdots, v_{i,\mathrm{D}}(k-P+1)]^T$ represents the ith subband noise vector at instant k. By substituting (13) into (8) and (9), the *a priori* error signal $\mathbf{e}_{i,\mathrm{D}}(k)$ and the *a posteriori* error signal $\boldsymbol{\xi}_{i,\mathrm{D}}(k)$ can be written as

$$\begin{aligned}\mathbf{e}_{i,\mathrm{D}}(k) &= \mathbf{d}_{i,\mathrm{D}}(k) - \mathbf{U}_i^T(k)\hat{\mathbf{w}}(k) \\ &= \mathbf{U}_i^T(k)\left(\mathbf{w}_{\mathrm{o}} - \hat{\mathbf{w}}(k)\right) + \mathbf{v}_{i,\mathrm{D}}(k),\end{aligned} \tag{14}$$

$$\begin{aligned}\boldsymbol{\xi}_{i,\mathrm{D}}(k) &= \mathbf{d}_{i,\mathrm{D}}(k) - \mathbf{U}_i^T(k)\hat{\mathbf{w}}(k+1) \\ &= \mathbf{U}_i^T(k)\left(\mathbf{w}_{\mathrm{o}} - \hat{\mathbf{w}}(k+1)\right) + \mathbf{v}_{i,\mathrm{D}}(k).\end{aligned} \tag{15}$$

By substituting (12) into (15), we have

$$\begin{aligned}\boldsymbol{\xi}_{i,\mathrm{D}}(k) = \mathbf{e}_{i,\mathrm{D}}(k) - \mu_i(k)\mathbf{U}_i^T(k)\mathbf{U}_i(k) \\ \times \left[\mathbf{U}_i^T(k)\mathbf{U}_i(k) + \delta\mathbf{I}\right]^{-1}\mathbf{e}_{i,\mathrm{D}}(k).\end{aligned} \tag{16}$$

In (15), given that the fullband adaptive filter approximates the unknown system, the subband *a posteriori* error is equal to the subband noise [8], namely,

$$\boldsymbol{\xi}_{i,\mathrm{D}}(k) = \mathbf{v}_{i,\mathrm{D}}(k). \tag{17}$$

However, subband noise cannot be obtained in several applications, such as AEC. Thus, the power of the subband noise should be estimated with a real-time approach. By taking the ℓ_2 norm of the vectors on both sides of (17), we obtain

$$E\left\{\left\|\boldsymbol{\xi}_{i,\mathrm{D}}(k)\right\|^2\right\} = E\left\{\left\|\mathbf{v}_{i,\mathrm{D}}(k)\right\|^2\right\}. \tag{18}$$

Substituting (16) into (18) yields

$$\begin{aligned}E\{||\mathbf{v}_{i,\mathrm{D}}(k)||^2\} = E\{||\mathbf{e}_{i,\mathrm{D}}(k)\{\mathbf{I} - \mu_i(k)\mathbf{U}_i^T(k)\mathbf{U}_i(k) \\ \times [\mathbf{U}_i^T(k)\mathbf{U}_i(k) + \delta\mathbf{I}]^{-1}\}||^2\}.\end{aligned} \tag{19}$$

Without any additional simplifications, $\mu_i(k)$ cannot be solved from (19). To make the problem tractable, we use two assumptions [12]. The first one is the simplification $\mathbf{U}_i^T(k)\mathbf{U}_i(k) \approx \|\mathbf{u}_i(k)\|^2\mathbf{I}$. The second one is that the fluctuations of $\|\mathbf{u}_i(k)\|^2$ are assumed to be small in one iteration. Then, (19) can be rewritten as

$$\begin{aligned}&E\left\{\left\|\mathbf{v}_{i,\mathrm{D}}(k)\right\|^2\right\} = \\ &\frac{\left(E\left\{\|\mathbf{u}_i(k)\|^2\right\} + \delta - \mu_i(k)E\left\{\|\mathbf{u}_i(k)\|^2\right\}\right)^2 E\left\{\|\mathbf{e}_{i,\mathrm{D}}(k)\|^2\right\}}{\left(E\left\{\|\mathbf{u}_i(k)\|^2\right\} + \delta\right)^2}.\end{aligned} \tag{20}$$

By solving (20), the formula of the *i*th subband step-size factor is as follows

$$\begin{aligned}\mu_i(k) &= \left(1-\sqrt{\frac{E\left\{\|\mathbf{v}_{i,\mathrm{D}}(k)\|^2\right\}}{E\left\{\|\mathbf{e}_{i,\mathrm{D}}(k)\|^2\right\}}}\right)\frac{E\left\{\|\mathbf{u}_i(k)\|^2\right\}+\delta}{E\left\{\|\mathbf{u}_i(k)\|^2\right\}} \\ &= \left(1-\frac{\sigma_{\mathbf{v}_{i,\mathrm{D}}}(k)}{\sigma_{\mathbf{e}_{i,\mathrm{D}}}(k)}\right)\frac{M\sigma^2_{\mathbf{u}_i}+\delta}{M\sigma^2_{\mathbf{u}_i}}\end{aligned} \tag{21}$$

where $\sigma^2_{\mathbf{v}_{i,\mathrm{D}}}(k) = E\left\{\|\mathbf{v}_{i,\mathrm{D}}(k)\|^2\right\}$, $\sigma^2_{\mathbf{e}_{i,\mathrm{D}}}(k) = E\left\{\|\mathbf{e}_{i,\mathrm{D}}(k)\|^2\right\}$ and $\sigma^2_{\mathbf{u}_i} = E\left\{\|u_i(k)\|^2\right\}$. In practice, the quantity $\sigma^2_{\mathbf{e}_{i,\mathrm{D}}}(k)$ can be estimated as follows

$$\sigma^2_{\mathbf{e}_{i,\mathrm{D}}}(k) = \alpha\sigma^2_{\mathbf{e}_{i,\mathrm{D}}}(k-1) + (1-\alpha)\|\mathbf{e}_{i,\mathrm{D}}(k)\|^2 \tag{22}$$

where $\alpha = 1 - N/(\kappa M)$ is a weighting factor, with $\kappa > 1$.

B. Estimations of Subband Noise Power

The power of the vector $\mathbf{v}_{i,\mathrm{D}}(k)$ must be estimated to calculate the variable step-size factor $\mu_i(k)$ in (21). A usual assumption is that the power of system noise can be easily estimated during silence [8]. However, this method has several limitations in practical applications because system noise could be time-variant and thus impossible to estimate in real time. Thus, the power of system noise may be biased. In the following, two real-time estimation methods are introduced to calculate the power of subband noise.

Iqbal *et al.* used a noise power estimation method based on the cross-correlation between the input signal and the *a priori* error signal [9]. Through this method, the power of subband noise can be estimated as follows

$$\sigma^2_{\mathbf{v}_{i,\mathrm{D}}}(k) = \sigma^2_{\mathbf{e}_{i,\mathrm{D}}}(k) - \frac{\mathbf{R}_i^T(k)\mathbf{R}_i(k)}{\sigma^2_{\mathbf{u}_{i,\mathrm{D}}}(k)} \tag{23}$$

where $\mathbf{R}_i(k) = \alpha\mathbf{R}_i(k-1) + (1-\alpha)\mathbf{U}_i(k)\mathbf{e}_{i,\mathrm{D}}(k)$ is the cross-correlation matrix and $\sigma^2_{\mathbf{u}_{i,\mathrm{D}}}(k)$ can be estimated as (22) similarly. When using the estimation method in (23), the variable step-size algorithm is called VSM-IMSAF-I.

Another estimation method proposed by Paleologu *et al.* is based on the assumption that the fullband filter vector has converged [10]. Thus, the echo signals can be approximated by the output signals of adaptive filter. Assuming that the subband noise and the echo signals $\mathbf{y}_{i,\mathrm{D}}(k)$ are uncorrelated, we have

$$\sigma^2_{\mathbf{v}_{i,\mathrm{D}}}(k) \approx \sigma^2_{\mathbf{d}_{i,\mathrm{D}}}(k) - \sigma^2_{\hat{\mathbf{y}}_{i,\mathrm{D}}}(k) \tag{24}$$

where $\hat{\mathbf{y}}_{i,\mathrm{D}}(k)$ indicates the output signal of the *i*th subband adaptive filter. Similarly, $\sigma^2_{\mathbf{d}_{i,\mathrm{D}}}(k)$ and $\sigma^2_{\hat{\mathbf{y}}_{i,\mathrm{D}}}(k)$ can be estimated as (22). When using the estimation method in (24), the variable step-size algorithm is called VSM-IMSAF-II. The performance of these two methods is compared in the following simulation.

C. Computational Complexity

The complexities of the proposed VSM-IMSAF-I and VSM-IMSAF-II algorithms are evaluated in this section. The sole difference between the proposed VSM algorithms and the standard IMSAF algorithm is in the calculation of the step size in (12). Table I presents the computational complexities of calculating the variable step size in the VSM-IMSAF-I and VSM-IMSAF-II algorithms. The complexity of VSM-IMSAF-I is much higher than that of VSM-IMSAF-II, particularly in several applications, such as AEC, in which the adaptive filter has thousands of coefficients. Several low-implementation schemes of the IMSAF algorithm can be found in [11], and they can be utilized in the proposed algorithms in a straightforward manner.

TABLE I
COMPUTATIONAL COMPLEXITIES OF CALCULATING VSM

	VSM-IMSAF-I	VSM-IMSAF-II
Additions	(*P*+1)*M*+2*P*+3	3*P*+3
Multiplications	(*P*+2)*M*+3*P*+4	3*P*+6
Divisions	2	1
Square-roots	1	1

IV. SIMULATION RESULTS

The VSM-IMSAF-I and VSM-IMSAF-II algorithms are evaluated in the context of system identification and AEC. $L = 512$ is the length of measured impulse response, and $M = 512$ is the length of adaptive filter. The sampling rate is 8 kHz. The analysis and synthesis filter banks consist of $N = 4$ channels of cosine modulated filters. AR(1) signals which has one pole at 0.9 and speech signals are used as input signals. The signal to noise ratio (SNR) of the near-end signal is 10 dB or 25 dB. Performance is evaluated with the normalized mean square deviation (NMSD) which is $10\log_{10}\left[\|\mathbf{w}_\mathrm{o} - \hat{\mathbf{w}}(k)\|^2 \Big/ \|\mathbf{w}_\mathrm{o}\|^2\right]$. When the input signals are AR(1) signals, the learning curves are the average of 50 trials. To satisfy the assumption in (24), the step-size factor of VSM-IMSAF-II is set to 1 in the initial *M* iterations.

Fig. 2 shows a comparison of the NMSD curves of the original IMSAF algorithm with $\mu = 0.8$ and $\mu = 0.11$ and two proposed VSM-IMSAF-I and VSM-IMSAF-II algorithms at SNR = 25 dB. As shown in Fig. 2, the performance of the IMSAF algorithm with a fixed step size depends on its step-size factor μ. When the step size $\mu = 0.8$, the convergence rate of the original IMSAF algorithm is fast but the steady-state misalignment is also high. When the step size $\mu = 0.11$, the steady-state misalignment of the original IMSAF algorithm is low, but the convergence rate is also slow. Both VSM-IMSAF-I and VSM-IMSAF-II algorithms can achieve more obvious advantages in convergence rate and steady-state misalignment than the original IMSAF algorithm.

Fig. 2 also displays the tracking performance of the three algorithms. At $t = 5.0s$, the echo path system $\mathbf{w}_\mathrm{o}$ is suddenly multiplied by -1. The change in the system can be quickly tracked by VSM-IMSAF-I and VSM-IMSAF-II. The reaction rate of VSM-IMSAF-II is slower than that of VSM-IMSAF-I. To explain the difference in reaction rate between VSM-IMSAF-I and VSM-IMSAF-II, we present the estimated noise power and step size in Fig. 3 in a single experiment for the 4th subband. As shown in from Fig. 3(a), at $t = 5.0 \sim 7.0s$ the estimated noise power of VSM-IMSAF-II is much larger than the true value. Due to the sudden change in impulse

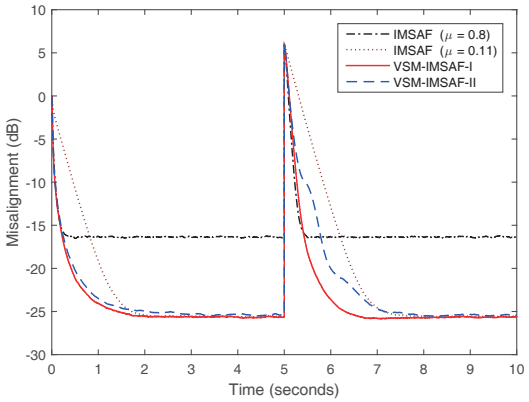

Fig. 2. Learning curves of IMSAF and VSM-IMSAF: $\delta = 15\sigma_u^2$, $N = 4$, $P = 2$, $L = M = 512$, $\kappa = 6$, SNR = 25 dB, AR(1) input.

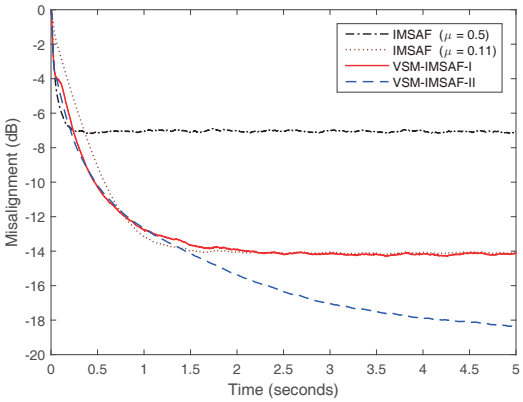

Fig. 4. Learning curves of IMSAF and VSM-IMSAF: $\delta = 15\sigma_u^2$, $N = 4$, $P = 2$, $L = M = 512$, $\kappa = 6$, SNR = 10 dB, AR(1) input.

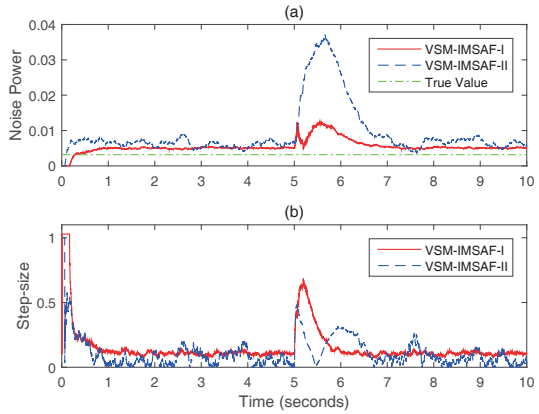

Fig. 3. Estimated noise power and step size of VSM-IMSAF: $\delta = 15\sigma_u^2$, $N = 4$, $P = 2$, $L = M = 512$, $\kappa = 6$, SNR = 25 dB, AR(1) input.

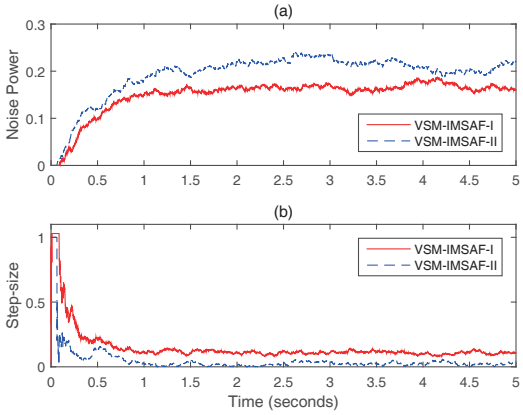

Fig. 5. Estimated noise power and step size of VSM-IMSAF: $\delta = 15\sigma_u^2$, $N = 4$, $P = 2$, $L = M = 512$, $\kappa = 6$, SNR = 10 dB, AR(1) input.

response $\mathbf{w}_o$ in this time interval, the assumption in (24) is not satisfied. The relationship between the step-size factor and subband noise power in (21) suggests that with the increase in subband noise power, the corresponding step size decreases. This result is in agreement with the result in Fig. 3(b), in which the step size of VSM-IMSAF-II is smaller than that of VSM-IMSAF-I after the unknown system changes. This explains that the tracking rate of VSM-IMSAF-II is slower than that of VSM-IMSAF-I.

Fig. 4 shows the NMSD curves for the three algorithms at a low SNR with 10 dB. Two fixed step-size factors are employed: $\mu = 0.5$ and $\mu = 0.11$. The other parameters are similar to those utilized in Fig. 2. The steady-state misalignment of VSM-IMSAF-II is lower than that of VSM-IMSAF-I by 4 dB. In Fig. 5, we also present the estimated noise power and variable step size for the 4th subband. As shown in Fig. 5(a), the estimated noise power of VSM-IMSAF-II is larger than that of VSM-IMSAF-I. Therefore, the step size of VSM-IMSAF-II is smaller than that of VSM-IMSAF-I according to (21), which is also confirmed by Fig. 5(b). The VSM-IMSAF-II algorithm has lower steady-state misalignment than the VSM-IMSAF-I algorithm at a low SNR.

Fig. 6 shows the NMSD curves for the three algorithms with a speech input signal. The projection order is $P = 4$ and two fixed step-size factors are utilized: $\mu = 1$ and $\mu = 0.2$. The other parameters are similar to those used in Fig. 2. As shown in Fig. 6, for the speech input signal, the proposed VSM-IMSAF-I and VSM-IMSAF-II algorithms have a conclusion similar to Fig. 2.

V. Conclusion

To resolve the conflict between convergence rate and steady-state misalignment of the original IMSAF algorithm, two variable step-size matrix IMSAF algorithms were developed in this study. Two real-time noise power estimation methods are adopted to calculate the variable step-size matrix. The performances of two algorithms are also analyzed. Computer simulations demonstrated that both VSM-IMSAF-I and VSM-IMSAF-II exhibit a significant improvement in convergence rate and steady-state misalignment. VSM-IMSAF-I achieves

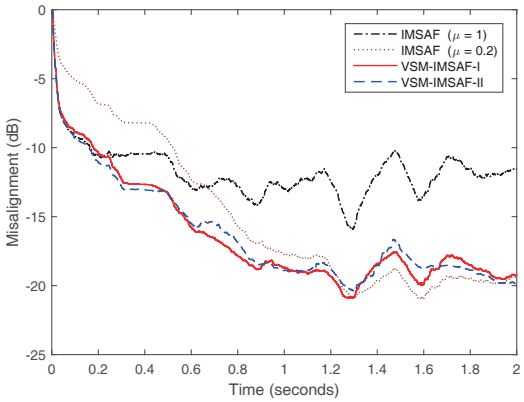

Fig. 6. Learning curves of the IMSAF and VSM-IMSAF: $\delta = 15\sigma_u^2$, $N = 4$, $P = 4$, $L = M = 512$, $\kappa = 6$, SNR = 25 dB, speech input.

more accurate estimated noise power and faster tracking rate than VSM-IMSAF-II, but the former has higher computational complexity.

ACKNOWLEDGMENT

This work was supported by National Natural Science Fund of China under Grant 61501449.

REFERENCES

[1] K. A. Lee, W. S. Gan, and S. M. Kuo, *Subband Adaptive Filtering: Theory and Implementation*. John Wiley & Sons, 2009.

[2] M. De Courville and P. Duhamel, "Adaptive filtering in subbands using a weighted criterion," *IEEE Trans. Signal Process.*, vol. 46, no. 9, pp. 2359-2371, Sept. 1998.

[3] S. S. Pradham and V. Reddy, "A new approach to subband adaptive filtering," *IEEE Trans. Signal Process.*, vol. 47, no. 3, pp. 655-664, Mar. 1999.

[4] V. DeBrunner, L. S. DeBrunner, and L. Wang, "Sub-band adaptive filtering with delay compensation for active control," *IEEE Trans. Signal Process.*, vol. 52, no. 10, pp. 2932-2937, Sept. 2004.

[5] K. A. Lee and W. S. Gan, "Improving convergence of the NLMS algorithm using constrained subband updates," *IEEE Signal Process. Lett.*, vol. 11, no. 9, pp. 736-739, Sept. 2004.

[6] F. Yang, M. Wu, P. Ji, and J. Yang, "An improved multiband-structured subband adaptive filter algorithm," *IEEE Signal Process. Lett.*, vol. 19, no. 10, pp. 647-650, Oct. 2012.

[7] F. Yang, M. Wu, P. Ji, Z. Kuang, and J. Yang, "Transient and steady-state analyses of the improved multiband-structured subband adaptive filter algorithm," *IET Signal Process.*, vol. 9, no. 8, pp. 596-604, Oct. 2015.

[8] J. Benesty, H. Rey, L. R. Vega, and S. Tressens, "A nonparametric VSS NLMS algorithm," *IEEE Signal Process. Lett.*, vol. 13, no. 10, pp. 581-584, Oct. 2006.

[9] M. A. Iqbal and S. L. Grant, "Novel variable step size NLMS algorithms for echo cancellation," in *Proc. IEEE Int. Conf. Acoust., Speech, Signal Process. (ICASSP)*, Las Vegas, NV, Apr. 2008, pp. 241-244.

[10] C. Paleologu, S. Ciochină, and J. Benesty, "Variable step-size NLMS algorithm for under-modeling acoustic echo cancellation," *IEEE Signal Process. Lett.*, vol. 15, no. 1, pp. 5-8, Jan. 2008.

[11] F. Yang, M. Wu, P. Ji, and J. Yang, "Low-complexity implementation of the improved multiband-structured subband adaptive filter algorithm," *IEEE Trans. Signal Process.*, vol. 63, no. 19, pp. 5133-5148, Sept. 2015.

[12] K. A. Lee, W. S. Gan, and S. M. Kuo, "Mean-square performance analysis of the normalized subband adaptive filter," in *Proc. 40th Asilomar Conf. Signals, Syst., Comput.*, Oct. 2006, pp. 248-252.